



HAL
open science

Jamming and metastability in one dimension: from the kinetically constrained Ising chain to the Riviera model

P. L. Krapivsky, J. M. Luck

► **To cite this version:**

P. L. Krapivsky, J. M. Luck. Jamming and metastability in one dimension: from the kinetically constrained Ising chain to the Riviera model. *The European Physical Journal. Special Topics*, 2023, 232 (11), pp.1703-1719. 10.1140/epjs/s11734-023-00804-w . cea-04211347

HAL Id: cea-04211347

<https://cea.hal.science/cea-04211347>

Submitted on 19 Sep 2023

HAL is a multi-disciplinary open access archive for the deposit and dissemination of scientific research documents, whether they are published or not. The documents may come from teaching and research institutions in France or abroad, or from public or private research centers.

L'archive ouverte pluridisciplinaire **HAL**, est destinée au dépôt et à la diffusion de documents scientifiques de niveau recherche, publiés ou non, émanant des établissements d'enseignement et de recherche français ou étrangers, des laboratoires publics ou privés.

Jamming and metastability in one dimension: from the kinetically constrained Ising chain to the Riviera model

P. L. Krapivsky¹ and J. M. Luck^{2*}

¹Department of Physics, Boston University, Boston, MA 02215, USA.

²Institut de Physique Théorique, Université Paris-Saclay, CNRS & CEA, 91191 Gif-sur-Yvette, France.

*Corresponding author(s). E-mail(s): jean-marc.luck@ipht.fr;
Contributing authors: pkrapivsky@gmail.com;

Abstract

The Ising chain with kinetic constraints provides many examples of totally irreversible zero-temperature dynamics leading to metastability with an exponentially large number of attractors. In most cases, the constrained zero-temperature dynamics can be mapped onto a model of random sequential adsorption. We provide a brief didactic review, based on the example of the constrained Glauber-Ising chain, of the exact results on the dynamics of these models and on their attractors that have been obtained by means of the above mapping. The Riviera model introduced recently by Puljiz et al. behaves similarly to the kinetically constrained Ising chains. This totally irreversible deposition model however does not enjoy the shielding property characterising models of random sequential adsorption. It can therefore neither be mapped onto such a model nor (in all likelihood) be solved by analytical means. We present a range of novel results on the attractors of the Riviera model, obtained by means of an exhaustive enumeration for smaller systems and of extensive simulations for larger ones, and put these results in perspective with the exact ones which are available for kinetically constrained Ising chains.

1 Introduction

The slow non-equilibrium dynamics of a broad variety of systems, including structural glasses, spin glasses and granular media, has often been modelled in terms of the motion of a particle in a multi-dimensional energy landscape with a great many valleys separated by barriers [1]. In mean-field models, barrier heights diverge in the thermodynamic limit, and so valleys become truly metastable states [2–4]. For finite-dimensional systems with short-range interactions, barrier heights

and valley lifetimes remain finite at any finite temperature, so that metastability becomes a matter of time scales [5–10].

Zero-temperature dynamics may also lead to metastability, in the broad sense that the system does not reach its ground state. Focussing for definiteness our attention onto spin models on finite-dimensional lattices, zero-temperature dynamics is known to lead to metastability in several instances. The two-dimensional ferromagnetic Ising model under zero-temperature Glauber dynamics may end in configurations with one or more frozen-in stripes [11, 12], whose statistics has been described via crossing probabilities in critical

percolation [13, 14]. On higher-dimensional lattices, the pattern of possible attractors is richer, including configurations with stochastic blinkers, i.e., clusters of spins which flip forever [11, 15]. The ferromagnetic spin chain under Glauber dynamics [16] reaches its ground state according to the coarsening paradigm [17], whereas zero-temperature Kawasaki dynamics yields metastability, in the sense that the energy of the blocked (or jammed) configurations reached by the dynamics is extensively above the ground-state energy [18, 19]. Spin chains endowed with zero-temperature single-spin-flip dynamics may also manifest metastability, at least in the following in two instances. In the presence of random ferromagnetic couplings, the spin chain has an exponentially large number of metastable configurations [20, 21]. On the other hand, preventing energy-preserving spin flips, and more generally imposing kinetic constraints, often leads to metastability. The latter situation is considered in detail below.

Kinetically constrained models have been introduced as the simplest systems of all exhibiting aging and many other features of the phenomenology of glassy dynamics [22]. For a broad range of one-dimensional kinetically constrained Ising models, zero-temperature dynamics exhibits metastability in the strong sense, with an exponentially large number of attractors, which are blocked (or jammed) configurations [23–36]. These attractors often have a simple local characterization in terms of forbidden patterns. As a consequence, the configurational entropy $S(E)$ [37, 38], such that the number of attractors at fixed energy density E grows as

$$\mathcal{N}(E) \sim \exp(NS(E)), \quad (1)$$

can be determined exactly, either by a direct combinatorial approach, by the transfer-matrix method used hereafter, or by a more recent renewal method [39], depending on the model.

Extended stochastic dynamical systems such as the above kinetically constrained models, having an exponentially large number of attractors, are usually strongly non ergodic. In particular, the energy density E_∞ at the end of the dynamics, where the system has settled into one of the many attractors which are at its disposal, depends continuously on the energy density E_0

of the initial state. One is then entitled to ask more detailed questions concerning the dynamical weights of attractors. If the system is launched from a random initial configuration with energy density E_0 , does it sample all attractors with energy density E_∞ with equal weights, i.e., with a flat measure, or, on the contrary, do the shape and size of the attraction basin of every single attractor matter? This question has been first addressed for slowly compacting granular matter. In this context, the assumption that the system explores its phase space with a flat measure is referred to as the Edwards hypothesis [40–43] (see [44] for a recent review).

The one-dimensional kinetically constrained Ising models investigated in [23–36] have the remarkable property that their zero-temperature dynamics can be mapped onto a model of random sequential adsorption (RSA) or cooperative sequential adsorption (CSA) [45–47], where identical objects are deposited sequentially and irreversibly on a substrate. These models are extensions of two well-known historical examples, the dimer deposition model on the chain solved by Flory [48] and the parking model on the continuous line solved by Rényi [49]. The constrained Ising chain reviewed in Section 2 maps onto Flory’s dimer deposition model. One-dimensional RSA and similar models enjoy a peculiar property dubbed shielding: the deposition of any elementary object splits the line into two half-lines whose future evolutions are independent from each other. The latter property ensures the exact solvability of this class of models, by means of a common analytical approach based on considering empty intervals. Many quantities concerning the dynamics of the system and its attractors can be derived in this way. Let us mention the dependence of the final energy density E_∞ on the initial one E_0 , which manifests the strong non-ergodicity of the dynamics, and the peculiarities of connected correlation functions, which generically exhibit oscillations and, more importantly, a superexponential, inverse-factorial fall-off. These results have established in particular that the Edwards hypothesis is in general not exactly valid for one-dimensional kinetically constrained models.

The goal of the present paper is to revisit the theory of one-dimensional spin models with kinetic constraints from a didactic viewpoint, and to use this body of knowledge to shed some

new light onto the Riviera model introduced recently [50]. The setup of this paper is as follows. In Section 2 we consider in detail the prototypical example of the kinetically constrained Ising chain, which can be mapped onto Flory's dimer deposition model. We successively review the various *a priori* statistical ensembles of attractors (Section 2.2) and the exact results that can be derived on the dynamics of the model and on the statistics of its attractors (Section 2.3). Section 3 is devoted to the Riviera model. The latter model is a one-dimensional variant, introduced recently by Puljiz et al. [50], of a two-dimensional irreversible deposition model introduced earlier by the same authors [51, 52]. Houses are sequentially built on an infinite array of pre-drawn plots along a beach, with the constraint that every house should enjoy the sunlight from at least one of the side directions. In other words, *at least one* of the two neighboring plots of each house should remain forever unbuilt. The strand is initially empty. New houses are successively introduced until a blocked configuration is reached. The above dynamical rule couples both neighboring sites of any occupied one. The Riviera model therefore does not enjoy the shielding property. The ensuing lack of exact solvability has observable consequences, including the exponential decay of the connected occupation correlation. We shall first consider the various *a priori* statistical ensembles of attractors (Section 3.2), and then present two kinds of results on the statistics of attractors, namely exact results obtained by enumeration on small systems (Section 3.3), and numerical results in the thermodynamic limit of very large systems (Section 3.4). Section 4 contains a discussion of our main findings.

2 The kinetically constrained Ising chain

2.1 Generalities

The reduced Hamiltonian of the ferromagnetic Ising chain reads

$$\mathcal{H} = - \sum_n \sigma_n \sigma_{n+1}, \quad (2)$$

where $\sigma_n = \pm 1$ are classical Ising spins living on the sites of the infinite chain.

To set the stage, the Ising chain is endowed with single-spin-flip dynamics, where each spin is flipped in continuous time at a rate $w(\delta\mathcal{H})$ depending only on the energy difference caused by the flip,

$$\delta\mathcal{H} = 2\sigma_n(\sigma_{n-1} + \sigma_{n+1}) \in \{-4, 0, +4\}. \quad (3)$$

Imposing detailed balance at inverse temperature β gives one single relation between the three rates, namely

$$w(+4) = e^{-4\beta} w(-4). \quad (4)$$

At zero temperature, we have $w(+4) = 0$, expressing that spin flips which would increase the energy are suppressed. Choosing time units such that $w(-4) = 1$, zero-temperature dynamics is therefore entirely characterized by the rate $w(0)$ of energy-conserving flips. For generic values of the latter rate, the model exhibits coarsening [17]. This is in particular the case for the historical example of Glauber dynamics [16], corresponding to $w(0) = 1/2$. The typical size of ferromagnetically ordered domains grows asymptotically as $L(t) \sim \sqrt{t}$, and so the energy density above the ground-state energy falls off as $1/\sqrt{t}$.

Energy-conserving flips are suppressed for the particular choice $w(0) = 0$. The descent dynamics thus obtained defines the kinetically constrained Ising chain. The only possible flips are those involving isolated spins:

$$-+- \rightarrow ---, \quad +-+ \rightarrow +++ \quad (5)$$

Isolated spins therefore flip once during their whole history, whereas other spins never flip. This is one of the simplest kinetically constrained models, which has been investigated at length in [31–36]. The main outcomes of these works will be reviewed in this section.

The descent dynamics of the constrained Ising chain can be recast as follows. We consider the dual lattice, where original bonds are mapped onto dual sites, and we encode satisfied (resp. unsatisfied) bonds as occupied (resp. empty) dual sites:

$$\begin{aligned} \bullet &: \tau_n = \sigma_n \sigma_{n+1} = +1, \\ \circ &: \tau_n = \sigma_n \sigma_{n+1} = -1, \end{aligned} \quad (6)$$

so that the Hamiltonian (2) reads

$$\mathcal{H} = - \sum_n \tau_n. \quad (7)$$

The spin flips (5) translate to

$$\circ\circ \rightarrow \bullet\bullet. \quad (8)$$

The constrained dynamics is thus mapped onto the dimer deposition model. The latter model, which has been first solved by Flory [48], is the simplest among all models in the RSA class. Attractors of the constrained Ising chain are in one-to-one correspondence with blocked configurations of the dimer deposition model. The energy density E of the Ising chain is related to the particle density ρ of the dimer model as

$$E = 1 - 2\rho. \quad (9)$$

We shall focus our attention onto the two-point energy correlation function

$$C_n = \langle \tau_0 \tau_n \rangle. \quad (10)$$

2.2 Statistical ensembles of attractors

In terms of the dimer deposition model, the attractors are all the configurations where empty sites are isolated. Equivalently, in terms of the Ising chain, there are no isolated spins. The statistical ensemble where all attractors are equally probable, according to a flat Edwards measure, is referred to as the full *a priori* ensemble, whereas the ensemble consisting of all attractors with fixed energy density E with equal weights is the microcanonical *a priori* ensemble.

2.2.1 Transfer-matrix formalism

As usual in statistical physics, instead of considering the microcanonical ensemble at fixed energy density E , it is advantageous to introduce the canonical ensemble defined by introducing an effective inverse temperature β conjugate to the Hamiltonian \mathcal{H} . For a finite chain of N sites, we thus introduce the partition function

$$Z_N = \sum_{\mathcal{C}} e^{-\beta \mathcal{H}(\mathcal{C})}, \quad (11)$$

where the sum runs over all blocked configurations \mathcal{C} of a system of N sites. The partial partition functions Z_N^\bullet and Z_N° , defined by assigning fixed values to the occupation of the rightmost site, obey linear recursions of the form

$$\begin{pmatrix} Z_{N+1}^\bullet \\ Z_{N+1}^\circ \end{pmatrix} = \mathbf{T} \begin{pmatrix} Z_N^\bullet \\ Z_N^\circ \end{pmatrix}, \quad (12)$$

involving the 2×2 transfer matrix

$$\mathbf{T} = \begin{pmatrix} e^\beta & e^\beta \\ e^{-\beta} & 0 \end{pmatrix}. \quad (13)$$

The eigenvalues of \mathbf{T} read

$$\lambda_\pm = \frac{1}{2} \left(e^\beta \pm \sqrt{4 + e^{2\beta}} \right). \quad (14)$$

An associated bi-orthogonal set of left and right eigenvectors, such that

$$\mathbf{L}_\pm \cdot \mathbf{R}_\pm = 1, \quad \mathbf{L}_\pm \cdot \mathbf{R}_\mp = 0, \quad (15)$$

reads

$$\mathbf{L}_\pm = \frac{(\lambda_\pm, e^\beta)}{\lambda_\pm^2 + 1}, \quad \mathbf{R}_\pm = \begin{pmatrix} \lambda_\pm \\ e^{-\beta} \end{pmatrix}. \quad (16)$$

2.2.2 Configurational entropy

The configurational entropy $S(E)$ introduced in (1) can be derived from the transfer-matrix formalism as follows. In the thermodynamic limit of a very large system size N , we have

$$\begin{aligned} Z_N &\approx \int \mathcal{N}(E) e^{-\beta N E} dE \\ &\sim \int e^{N(S(E) - \beta E)} dE \\ &\sim e^{N \ln \lambda_+(\beta)}. \end{aligned} \quad (17)$$

We thus find that $S(E)$ is the Legendre transform of $\ln \lambda_+(\beta)$, i.e.,

$$S(E) = \ln \lambda_+(\beta) + \beta E, \quad (18)$$

with

$$\beta = \frac{dS}{dE}, \quad E = -\frac{d \ln \lambda_+}{d\beta}. \quad (19)$$

The above relations are germane to the usual thermodynamic ones between internal energy E and

free energy $F = E - TS$. Using (14), we obtain the expressions

$$E = -\frac{e^\beta}{\sqrt{4 + e^{2\beta}}}, \quad e^\beta = -\frac{2E}{\sqrt{1 - E^2}}, \quad (20)$$

and

$$\begin{aligned} S(E) &= \frac{1}{2}(1 - E) \ln(1 - E) \\ &\quad - \frac{1}{2}(1 + E) \ln(1 + E) \\ &\quad + E \ln(-2E). \end{aligned} \quad (21)$$

The configurational entropy $S(E)$ is plotted against the energy density E in Figure 1. It vanishes at both endpoints $E_{\min} = -1$ and $E_{\max} = 0$. Its maximum, corresponding to $\beta = 0$, namely

$$S_\star = \ln \frac{\sqrt{5} + 1}{2} \approx 0.481212, \quad (22)$$

is reached for

$$E_\star = -\frac{\sqrt{5}}{5} \approx -0.447214. \quad (23)$$

The above number is therefore the *a priori* most probable value of the energy density of an attractor of the Ising chain.

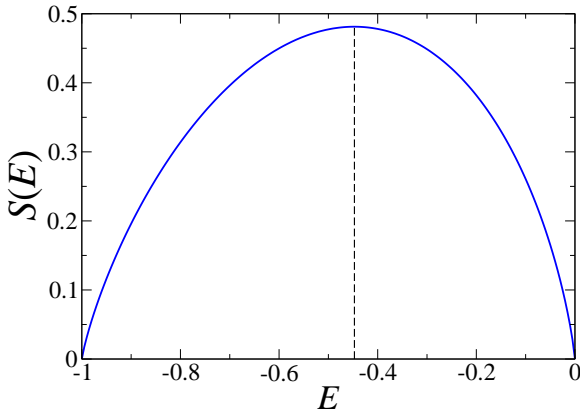


Fig. 1 Configurational entropy $S(E)$ of the constrained Ising chain, as given in (21), against energy density E of attractors (blocked configurations). Vertical dashed line: *a priori* energy density E_\star yielding the maximum configurational entropy S_\star (see (22), (23)).

Another interpretation of the configurational entropy $S(E)$ is as follows. The *a priori* probability $P(E)$ of observing in the full statistical

ensemble a blocked configuration with an atypical energy density $E \neq E_\star$ is given by a large-deviation formula of the form

$$P(E) \sim \exp(-N\Sigma(E)), \quad (24)$$

where the *a priori* large-deviation function reads

$$\Sigma(E) = S_\star - S(E). \quad (25)$$

This quantity is positive and vanishes quadratically in the vicinity of $E = E_\star$.

2.2.3 Correlation function

The expression $C_{n,\text{mic}}$ of the two-point correlation introduced in (10) in the microcanonical *a priori* ensemble at fixed energy density E can also be derived from the transfer-matrix formalism. We have for $n \geq 0$

$$C_{n,\text{mic}} = \lim_{M,N \rightarrow \infty} \frac{\text{tr } \mathbf{T}^M \mathbf{E} \mathbf{T}^n \mathbf{E} \mathbf{T}^N}{\text{tr } \mathbf{T}^{M+n+N}}, \quad (26)$$

i.e.,

$$\begin{aligned} C_{n,\text{mic}} &= \frac{\mathbf{L}_+ \cdot \mathbf{E} \mathbf{T}^n \mathbf{E} \mathbf{R}_+}{\lambda_+^n}, \\ &= (\mathbf{L}_+ \cdot \mathbf{E} \mathbf{R}_+)^2 \\ &\quad + (\mathbf{L}_+ \cdot \mathbf{E} \mathbf{R}_-)(\mathbf{L}_- \cdot \mathbf{E} \mathbf{R}_+) \left(\frac{\lambda_-}{\lambda_+}\right)^n. \end{aligned} \quad (27)$$

According to the equivalence between statistical ensembles, the transfer matrix \mathbf{T} , its largest eigenvalue λ_+ , and the associated eigenvectors \mathbf{L}_+ and \mathbf{R}_+ are evaluated at the effective inverse temperature β related to the energy density E by (20). The diagonal matrix

$$\mathbf{E} = \begin{pmatrix} -1 & 0 \\ 0 & 1 \end{pmatrix} \quad (28)$$

is the energy operator.

Using (14), (15), (16), as well as

$$\mathbf{L}_\pm \cdot \mathbf{E} \mathbf{R}_\pm = \pm E, \quad \mathbf{L}_\pm \cdot \mathbf{E} \mathbf{R}_\mp = 1 \pm E, \quad (29)$$

we are left with the simple result

$$C_{n,\text{mic}} = E^2 + (1 - E^2) \left(\frac{1 + E}{1 - E}\right)^n. \quad (30)$$

The disconnected part of the above correlation is the square of the energy density E , as should be. The connected part exhibits exponentially damped oscillations.

2.3 Exact results on dynamics and attractors

In this section we review, on the example of the constrained Ising chain whose dynamics can be mapped onto the dimer deposition model [31–36], the approach yielding exact analytical results on the dynamics and the attractors of RSA models in one dimension (see [45–47] for reviews).

We consider a factorized initial state where each variable τ_n is chosen at random as

$$\begin{aligned} \tau_n = -1 (\circ) & \quad \text{with prob. } p, \\ \tau_n = +1 (\bullet) & \quad \text{with prob. } 1 - p, \end{aligned} \quad (31)$$

so that the energy density of the Ising chain and the particle density of the dimer model read

$$E(0) = E_0 = 2p - 1, \quad \rho(0) = \rho_0 = 1 - p. \quad (32)$$

In particular, $p = 1$ corresponds to the dimer system being initially empty, whereas $p = 1/2$ corresponds to an infinite-temperature initial state for the Ising chain.

2.3.1 Energy density

The temporal evolution of thermodynamic quantities such as the energy density $E(t)$ can be derived by analytical means by using the shielding property of one-dimensional RSA and germane problems, implying that the densities of empty intervals obey closed evolution equations. In terms of the dimer deposition model, let

$$p_\ell(t) = \text{Prob}(\underbrace{\bullet \circ \cdots \circ \bullet}_\ell) \quad (33)$$

denote the density per unit length at time t of intervals consisting of exactly ℓ consecutive empty sites, with $\ell \geq 1$, so that we have

$$E(t) = 1 - 2\rho(t), \quad \rho(t) = 1 - \sum_{\ell \geq 1} \ell p_\ell(t). \quad (34)$$

The probabilities $p_\ell(t)$ obey evolution equations which can be derived as follows. Clusters of length

$\ell = 1$ are inactive, whereas a new dimer can be deposited at $(\ell - 1)$ places on a cluster of length $\ell \geq 2$. We thus arrive to the coupled linear differential equations

$$\frac{dp_\ell(t)}{dt} = -(\ell - 1)p_\ell(t) + 2 \sum_{k \geq \ell + 2} p_k(t) \quad (35)$$

for $\ell \geq 1$, with initial condition

$$p_\ell(0) = (1 - p)^2 p^\ell. \quad (36)$$

Inserting an Ansatz of the form $p_\ell(t) = a(t)z(t)^\ell$ into (35) yields two differential equations for $z(t)$ and $a(t)$. We thus obtain

$$p_\ell(t) = (1 - pe^{-t})^2 \exp(2p(e^{-t} - 1)) p^\ell e^{-(\ell - 1)t}, \quad (37)$$

and so

$$\begin{aligned} E(t) &= 2p \exp(2p(e^{-t} - 1)) - 1, \\ \rho(t) &= 1 - p \exp(2p(e^{-t} - 1)). \end{aligned} \quad (38)$$

In the limit of infinitely long times, only inactive intervals of length $\ell = 1$ survive, as should be. Their limiting density reads

$$p_1(t \rightarrow \infty) = pe^{-2p}, \quad (39)$$

and so

$$E_\infty = 2pe^{-2p} - 1, \quad \rho_\infty = 1 - pe^{-2p} \quad (40)$$

are respectively the final energy and particle densities in the blocked configurations.

For an initially empty system ($p = 1$), the final density (or coverage) of the dimer deposition model reads

$$\rho_\infty = 1 - e^{-2} \approx 0.864664. \quad (41)$$

This is the celebrated result of Flory [48].

Using (32) and (40), the final energy density E_∞ of the constrained Ising chain can be expressed as a function of its initial energy density E_0 , namely

$$E_\infty = (E_0 + 1)e^{-E_0 - 1} - 1. \quad (42)$$

The final energy E_∞ is plotted against E_0 in Figure 2. It is significantly lower than the *a priori*

value (23), and lower than E_0 , as should be. Furthermore, it exhibits a non-monotonic dependence on E_0 . Near the ground-state energy ($E_0 \rightarrow -1$), we have $E_\infty - E_0 \approx (E_0 + 1)^2$. The final energy increases to the maximal value

$$E_\infty = e^{-1} - 1 \approx -0.632120 \quad (43)$$

for $E_0 = 0$, i.e., an infinite-temperature initial state, and then decreases to the value

$$E_\infty = 2e^{-2} - 1 \approx -0.729329 \quad (44)$$

for $E_0 = 1$, i.e., an antiferromagnetically ordered initial state.

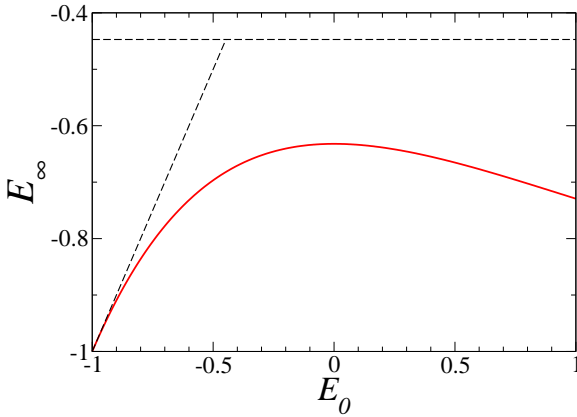


Fig. 2 Final energy density E_∞ of the constrained Ising chain, as given in (42), against initial energy density E_0 . Oblique dashed line: diagonal ($E_\infty = E_0$). Horizontal dashed line: *a priori* value (23).

2.3.2 Energy correlation function

The temporal evolution of the two-point correlation introduced in (10) can also be obtained by using the shielding property. The derivation involves the following one-cluster and two-cluster functions

$$c_n(t) = \text{Prob}(\underbrace{\circ \dots \circ}_n),$$

$$d_{m,k,n}(t) = \text{Prob}(\underbrace{\circ \dots \circ}_m \dots \underbrace{\circ \dots \circ}_k \dots \underbrace{\circ \dots \circ}_n), \quad (45)$$

where the contents of the middle interval of length k is unspecified. The above functions obey

the coupled linear equations

$$\begin{aligned} \frac{dc_n(t)}{dt} &= -(n-1)c_n(t) - 2c_{n+1}(t), \quad (46) \\ \frac{dd_{m,k,n}(t)}{dt} &= -(m+n-2)d_{m,k,n}(t) \\ &\quad - d_{m+1,k,n}(t) - d_{m,k,n+1}(t) \\ &\quad - d_{m+1,k-1,n}(t) - d_{m,k-1,n+1}(t), \end{aligned}$$

with appropriate initial and boundary conditions.

Skipping details, we mention the expression of the final connected correlation ($n \geq 1$) [35]:

$$\begin{aligned} C_{n,\infty} - E_\infty^2 &= 2pe^{-2p} \frac{(-2p)^n}{n!} \\ &\quad - 4p^2 e^{-2p} \sum_{m \geq n} \frac{(-2p)^m}{m!}. \quad (47) \end{aligned}$$

This result exhibits the generic features of connected correlations in RSA model already mentioned in the Introduction [45–47], including oscillations and, more importantly, an inverse-factorial fall-off. This peculiar kind of superexponential decay seems to have been evidenced first in [53] (see [54, 55] for alternative derivations).

Figure 3 shows a comparison between the final connected correlation $C_{n,\infty} - E_\infty^2$, given by (47), and its counterpart $C_{n,\text{mic}} - E_\infty^2$ in the *a priori* microcanonical ensemble at fixed energy E (see (30)). In order for the comparison to be fair, the exact final energy E_∞ has been used to define the *a priori* ensemble. Data corresponding to an infinite-temperature initial state, i.e., $p = 1/2$ or $E_0 = 0$, so that E_∞ is given by (43), are plotted on a logarithmic scale against distance n . The microcanonical ensemble correctly predicts $C_{0,\text{mic}} = C_{0,\infty} = 1$, by construction, as well as $C_{1,\text{mic}} = C_{1,\infty} = -2E_\infty - 1$. The two datasets cross each other between distances 5 and 6. The superexponential decay of the exact correlations is clearly visible.

2.3.3 Dynamical entropy

The above method can be further extended to derive an exact expression for the full dynamical entropy function $\Sigma_\infty(E)$, such that the probability $P_\infty(E)$ of observing a final blocked configuration with an atypical energy density $E \neq E_\infty$ is given

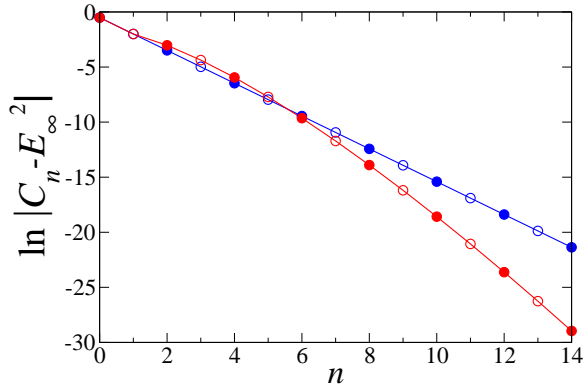


Fig. 3 Comparison between the final connected correlation $C_{n,\infty} - E_{\infty}^2$, given by (47) (red symbols) and its counterpart $C_{n,\text{mic}} - E_{\infty}^2$ in the *a priori* microcanonical ensemble at fixed energy E (see (30)) (aligned blue symbols). Data are plotted on a logarithmic scale against distance n . They correspond to $p = 1/2$ or $E_0 = 0$, and so E_{∞} is given by (43). Full (resp. empty) symbols denote positive (resp. negative) connected correlations.

by a large-deviation formula of the form

$$P_{\infty}(E) \sim \exp(-N\Sigma_{\infty}(E)). \quad (48)$$

The calculations involved in the derivation of dynamical large-deviation functions in RSA models [35, 36, 56] are more intricate than those exposed in Sections 2.3.1 (energy density) and 2.3.2 (energy correlation).

Skipping every detail, we mention that the dynamical entropy of the constrained Ising chain is given by the following parametric form [35]:

$$\begin{aligned} \Sigma_{\infty} &= \ln z + \frac{(1 + (2p - 1)z)^2 - (1 - z)^2 e^{4pz}}{4pz^2 e^{2pz} (2(1 - p) + (2p - 1)z)} \\ &\quad \times \ln \frac{1 + (2p - 1)z + (1 - z)e^{2pz}}{1 + (2p - 1)z - (1 - z)e^{2pz}}, \\ E &= \frac{(1 + (2p - 1)z)^2 - (1 - z)^2 e^{4pz}}{2pz^2 e^{2pz} (2(1 - p) + (2p - 1)z)} - 1, \end{aligned} \quad (49)$$

where the parameter z runs between zero and a positive maximal value z_c such that

$$1 + (2p - 1)z_c + (1 - z_c)e^{2pz_c} = 0. \quad (50)$$

The dynamical entropy $\Sigma_{\infty}(E)$ is positive, vanishes quadratically in the vicinity of $E = E_{\infty}$, and has finite limits at both endpoints, namely

$$\Sigma_{\infty}(-1) = \ln z_c,$$

$$\Sigma_{\infty}(0) = -\frac{1}{2} \ln(p(1 - p)). \quad (51)$$

Figure 4 shows a comparison between the dynamical entropy $\Sigma_{\infty}(E)$ given in (49), for $p = 1/2$, corresponding to $E_0 = 0$, i.e., an infinite-temperature initial state, and the *a priori* large-deviation function $\Sigma(E)$, given in (25). Both quantities are plotted against the energy density E . Their endpoint values read $\Sigma_{\infty}(-1) = \ln z_c \approx 0.245659$, $\Sigma_{\infty}(0) = \ln 2 \approx 0.693147$, $\Sigma(-1) = \Sigma(0) = S_{\star} \approx 0.481211$.

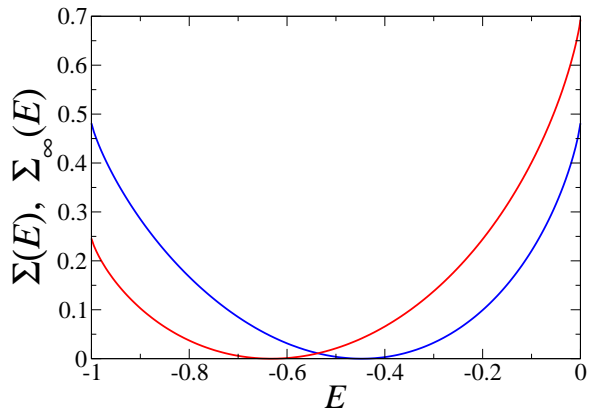


Fig. 4 Red curve: dynamical entropy $\Sigma_{\infty}(E)$ given in (49) for $p = 1/2$, corresponding to $E_0 = 0$, i.e., an infinite-temperature initial state. Blue curve: *a priori* large-deviation function $\Sigma(E)$ given in (25). Both quantities are plotted against the energy density E .

3 The Riviera model

3.1 Definition

The Riviera model is the one-dimensional variant introduced recently by Puljiz et al. [50] of a two-dimensional irreversible deposition model introduced earlier by the same authors [51, 52]. Houses are sequentially built on plots of equal sizes along an infinitely long beach, to be viewed as the sites of an infinite chain, with the constraint that every house should enjoy the sunlight from at least one of the side directions. In other words *at least one* of the two neighboring plots of each house should remain forever unbuild. The strand is initially empty. New houses are introduced until a block configuration is reached. Here is a blocked configuration on a system of length 40, comprising

We denote by \mathbf{L}_a and \mathbf{R}_a the left and right eigenvectors associated with λ_a , normalized so as to have $\mathbf{L}_a \cdot \mathbf{R}_b = \delta_{ab}$.

The parametrization (61), (62) implies the following symmetry. Changing u into $1/u$ leaves x invariant and changes λ into x/λ . Therefore, for any fixed x , if λ is an eigenvalue of \mathbf{T} , corresponding to the parameter u , x/λ is another eigenvalue, corresponding to the parameter $1/u$. The transfer matrix \mathbf{T} has degenerate eigenvalues in two cases: $x = 0$, where the six eigenvalues collapse to the origin, and

$$x_c = \frac{256}{27} \approx 9.481481, \quad (63)$$

where \mathbf{T} has a pair of twice degenerate complex eigenvalues. In the most relevant range $x < x_c$, the structure of the spectrum of \mathbf{T} is shown in Figure 5. The largest eigenvalue λ_1 and the smallest one $\lambda_2 = x/\lambda_1$ are real positive, whereas the four other eigenvalues $\lambda_3, \dots, \lambda_6$ form two complex conjugate pairs, with negative real parts and common modulus \sqrt{x} . For $x > x_c$, one pair of complex eigenvalues have modulus less than \sqrt{x} , whereas the other pair has modulus greater than \sqrt{x} .

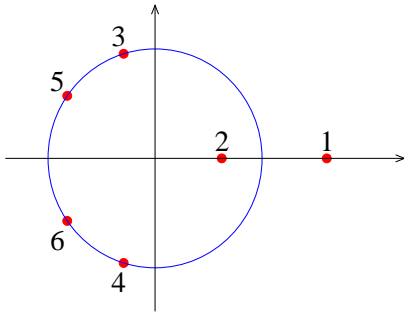


Fig. 5 Structure of the spectrum of the transfer matrix \mathbf{T} for $x < x_c$. Red symbols: eigenvalues λ_a labelled by $a = 1, \dots, 6$. The blue circle centered at the origin with radius \sqrt{x} contains the four complex eigenvalues.

3.2.2 Statistics of finite systems

Before we investigate the configurational entropy and correlations in the thermodynamic limit, let us focus our attention onto finite systems.

The number $\mathcal{N}_{N,M}$ of distinct blocked configurations comprising M houses on a finite system

of N sites can be derived from the transfer-matrix formalism as follows. The partition function

$$Z_N(x) = \sum_M \mathcal{N}_{N,M} x^M \quad (64)$$

is given by the linear combination corresponding to open boundary conditions at both ends of the partial partition functions obeying the recursion (57). Some algebra yields the expression

$$Z_N(x) = \mathbf{L}_{\text{open}} \cdot \mathbf{T}^N \mathbf{R}_{\text{open}}, \quad (65)$$

with

$$\begin{aligned} \mathbf{L}_{\text{open}} &= (0 \ 0 \ 1 \ 0 \ 1 \ 1), \\ \mathbf{R}_{\text{open}} &= (0 \ 0 \ 0 \ 0 \ 0 \ 1)^T, \end{aligned} \quad (66)$$

where the superscript T denotes transposition. The total number of distinct blocked configurations on a system of size N reads

$$\mathcal{N}_N = \sum_M \mathcal{N}_{N,M} = Z_N(1). \quad (67)$$

The partition functions $Z_N(x)$ and the numbers \mathcal{N}_N obey the linear recursions

$$\begin{aligned} Z_{N+6}(x) - xZ_{N+4}(x) - x^2(Z_{N+3}(x) + Z_{N+2}(x)) \\ + x^3Z_N(x) = 0 \end{aligned} \quad (68)$$

and

$$\mathcal{N}_{N+6} - \mathcal{N}_{N+4} - \mathcal{N}_{N+3} - \mathcal{N}_{N+2} + \mathcal{N}_N = 0, \quad (69)$$

as a consequence of the characteristic equation (60).

An elegant presentation of the above results in terms of their generating series has been given in [50]. With the present notations, we have

$$\begin{aligned} \mathcal{Z}(x, y) &= \sum_{M,N} \mathcal{N}_{N,M} x^M y^N \\ &= \sum_{N \geq 0} Z_N(x) y^N \\ &= \mathbf{L}_{\text{open}} \cdot (1 - y\mathbf{T})^{-1} \mathbf{R}_{\text{open}} \quad (70) \\ &= \frac{1 + xy + x(x-1)y^2 + x^2y^3 - x^3y^5}{1 - xy^2 - x^2(y^3 + y^4) + x^3y^6} \end{aligned}$$

and

$$\begin{aligned} z(y) &= \sum_{N \geq 0} \mathcal{N}_N y^N \\ &= \mathcal{Z}(1, y) \\ &= \frac{1 + y + y^3 - y^5}{1 - y^2 - y^3 - y^4 + y^6}. \end{aligned} \quad (71)$$

The above results have also been put in perspective with several combinatorial problems in [50]. In particular, the numbers \mathcal{N}_N of blocked configurations count a class of permutations with strongly restricted displacements. They are listed in the OEIS under reference A080013 [57] (see also [58]).

Table 1 gives the expression of the partition function $Z_N(x)$ and the total number \mathcal{N}_N of blocked configurations for sizes N up to 14. The last line means that, on a system of $N = 14$ sites, there are altogether 91 distinct blocked configurations, among which 50 have $M = 8$ houses, 40 have $M = 9$ and a single one has $M = 10$, namely

●●●●●●●●●●●●●●.

N	$Z_N(x)$	\mathcal{N}_N
0	1	1
1	x	1
2	x^2	1
3	$3x^2$	3
4	$x^2 + 2x^3$	3
5	$3x^3 + x^4$	4
6	$6x^4$	6
7	$6x^4 + 3x^5$	9
8	$x^4 + 10x^5 + x^6$	12
9	$6x^5 + 10x^6$	16
10	$20x^6 + 4x^7$	24
11	$10x^6 + 22x^7 + x^8$	33
12	$x^6 + 30x^7 + 15x^8$	46
13	$10x^7 + 49x^8 + 5x^9$	64
14	$50x^8 + 40x^9 + x^{10}$	91

Table 1 Partition functions $Z_N(x)$ of finite systems of N sites, for N up to 14. The quantity $\mathcal{N}_N = Z_N(1)$ is the total number of distinct blocked configurations on a system of size N .

The mean particle density $\rho_{N,\star}$ in the *a priori* ensemble where all blocked configurations of the finite system of size N are equally probable reads

$$\rho_{N,\star} = \frac{1}{NZ_N} \left(\frac{dZ_N}{dx} \right)_{x=1}. \quad (72)$$

The rational values of the *a priori* densities $\rho_{N,\star}$ will be given in Table 3, for N up to 14, together with their dynamical analogues $\rho_{N,\infty}$, defined in (89).

3.2.3 Configurational entropy

The configurational entropy $S(\rho)$ is given by (18), (19), up to the replacement of the energy density E by the particle density ρ , and of λ_+ by the largest eigenvalue λ_1 of \mathbf{T} . With the parametrization (61), (62), λ_1 is reached for u real in the range $1 < u < +\infty$. We thus obtain the following parametric representation of the configurational entropy:

$$\rho = \frac{2u^2 + u + 1}{D}, \quad (73)$$

$$S = \frac{A}{D}, \quad (74)$$

$$\begin{aligned} A &= u(3u + 1) \ln u \\ &\quad - (u^2 - 1) \ln((u - 1)^2(u + 1)), \end{aligned} \quad (75)$$

$$D = 3u^2 + 2u + 3. \quad (76)$$

The configurational entropy $S(\rho)$ is plotted in Figure 6 against the particle density ρ . It vanishes at the endpoints $\rho_{\min} = 1/2$ and $\rho_{\max} = 2/3$, respectively corresponding to the periodic patterns ●●●●●●●● and ●●●●●●●●. The maximum of the configurational entropy,

$$S_\star \approx 0.337377, \quad (77)$$

is reached for $\beta = 0$, i.e., $x = 1$. The corresponding values of u and ρ read

$$u_\star \approx 1.963553, \quad \rho_\star \approx 0.577203. \quad (78)$$

The above value of ρ_\star represents the most probable particle density in the full *a priori* statistical ensemble.

3.2.4 Correlation function

The expression $C_{n,\text{mic}}$ of the occupation correlation introduced in (54) in the microcanonical *a priori* ensemble at fixed density ρ can be derived from the transfer-matrix formalism along the lines of Section 2.2.

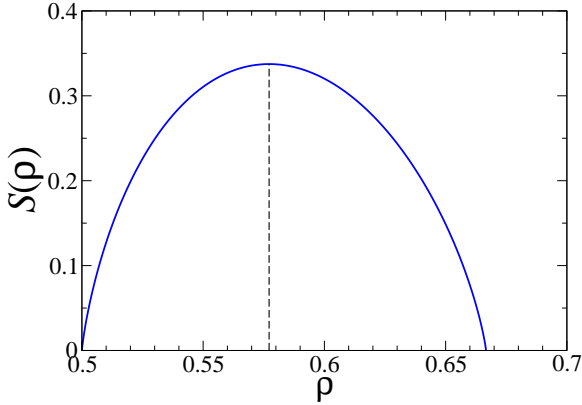


Fig. 6 Configurational entropy $S(\rho)$ of the Riviera model, as given in (74), against particle density ρ of blocked configurations. Vertical dashed line: most probable density ρ_* yielding the maximum configurational entropy S_* (see (77), (78)).

In analogy with (27), we have for $n \geq 0$

$$C_{n,\text{mic}} = \frac{B_n}{\lambda_+^n}, \quad (79)$$

with

$$B_n = \mathbf{L}_1 \cdot \mathbf{Y} \mathbf{T}^n \mathbf{Y} \mathbf{R}_1 \quad (80)$$

$$= \sum_{a=1}^6 (\mathbf{L}_1 \cdot \mathbf{Y} \mathbf{R}_a) (\mathbf{L}_a \cdot \mathbf{Y} \mathbf{R}_1) \lambda_a^n. \quad (81)$$

Here again, the transfer matrix \mathbf{T} and its eigenvalues and eigenvectors are evaluated at the effective inverse temperature β related to the density ρ by (59), (61), (73). The diagonal matrix

$$\mathbf{Y} = \begin{pmatrix} 1 & 0 & 0 & 0 & 0 & 0 \\ 0 & 0 & 0 & 0 & 0 & 0 \\ 0 & 0 & 1 & 0 & 0 & 0 \\ 0 & 0 & 0 & 0 & 0 & 0 \\ 0 & 0 & 0 & 0 & 1 & 0 \\ 0 & 0 & 0 & 0 & 0 & 0 \end{pmatrix} \quad (82)$$

is the occupation operator. We have consistently $\mathbf{L}_1 \cdot \mathbf{Y} \mathbf{R}_1 = \rho$, so that the term with $a = 1$ in (81) yields the expected disconnected component of the correlation, namely ρ^2 .

The expression (80) for the numerators B_n implies that they obey the same linear recursion as the partition functions $Z_N(x)$ (see (68)), i.e.,

$$B_{n+6} - x B_{n+4} - x^2 (B_{n+3} + B_{n+2})$$

$$+ x^3 B_n = 0. \quad (83)$$

With the parametrization (61), (62), the recursion (83) translates to a recursion relation for the microcanonical correlations $C_{n,\text{mic}}$ themselves:

$$\begin{aligned} u^3 C_{n+6,\text{mic}} - u^2 C_{n+4,\text{mic}} \\ - (u-1)^2 (u+1) C_{n+3,\text{mic}} \\ - u C_{n+2,\text{mic}} + C_{n,\text{mic}} = 0. \end{aligned} \quad (84)$$

The above recursion allows one to determine recursively the correlations at all distances from the following first six values

$$\begin{aligned} C_{0,\text{mic}} &= \rho = \frac{2u^2 + u + 1}{D}, \\ C_{1,\text{mic}} &= \frac{u^2}{D}, \\ C_{2,\text{mic}} &= \frac{u(u+1)}{D}, \\ C_{3,\text{mic}} &= \frac{2u^2 - 1}{D}, \\ C_{4,\text{mic}} &= \frac{u^3 + 2u + 1}{uD}, \\ C_{5,\text{mic}} &= \frac{(u^2 + u - 1)^2}{u^2 D}, \end{aligned} \quad (85)$$

which can be derived from (79), (80) by means of computer algebra. The denominator D has been given in (76).

The numerators of the first four correlations in (85) are quadratic in u . These quantities therefore obey two linear identities, which can be written as

$$\begin{aligned} C_2 &= 3\rho - 2C_1 - 1, \\ C_3 &= 2\rho + C_1 - 1. \end{aligned} \quad (86)$$

All ‘mic’ subscripts have been suppressed in the above equations for the following reason. These identities have been derived within the microcanonical framework, irrespective of the parameter u , i.e., irrespective of the mean density ρ . It will be shown below that these are constitutive identities, which ensue from the mere structure of the blocked configurations. In particular, the above identities hold for the final correlations $C_{n,\infty}$.

The large-distance behavior of the connected correlation is dominated by the terms with $a =$

3, . . . , 6 in (81), involving the four complex eigenvalues of \mathbf{T} . The phases of the latter eigenvalues are generically not rationally related to π . The connected correlations therefore exhibit everlasting quasiperiodic oscillations, whose hull falls off exponentially as

$$C_{n,\text{mic}} - \rho^2 \sim e^{-\mu n}. \quad (87)$$

For $x < x_c$, the structure of the spectrum shown in Figure 5 implies

$$\mu = \ln \frac{\lambda_1}{\sqrt{x}} = \frac{1}{2} \ln u. \quad (88)$$

3.3 Exact results on the attractors of finite systems

In the dynamics of the Riviera model, sites (i.e., plots of land) are visited in a random sequential order. The totally irreversible rules of the model ensure that a house may be built at a given site only at the first time this site is visited, whereas any subsequent visit is doomed to be sterile.

For an initially empty finite system of N sites, the attractor reached by a given realization of the process therefore only depends on the order in which the various sites are visited for the first time. It is advantageous to encode this ordering by a permutation σ of the N site labels ($i = 1, \dots, N$), such that site σ_1 is visited first, and so on, until site σ_N is visited last. There are $N!$ distinct permutations, and therefore $N!$ equally probable distinct realizations of the Riviera process. It is natural to define the dynamical weight $W(\mathcal{C})$ of each attractor \mathcal{C} as being the number of permutations for which the system ends up in the blocked configuration \mathcal{C} . An analogous approach based on uniform random permutations has already been used in earlier work [59].

For moderate values of the system size N , the $N!$ permutations can be enumerated and the corresponding dynamics be run by means of a computer routine, yielding the dynamical weights of all attractors of the model, and therefore the exact values of all observables defined in terms of those attractors. In particular, the mean final particle density on a system of size N reads

$$\rho_{N,\infty} = \frac{1}{N N!} \sum_{\mathcal{C}} W(\mathcal{C}) M(\mathcal{C}), \quad (89)$$

where the sum runs over all blocked configurations \mathcal{C} of size N , $W(\mathcal{C})$ is the dynamical weight of \mathcal{C} defined above, and $M(\mathcal{C})$ is the number of occupied sites (i.e., houses) in \mathcal{C} .

Table 2 gives the dynamical weights $W(\mathcal{C})$ of all attractors of the Riviera model, as obtained by means of the above enumeration approach, ordered by increasing values of system size N and number M of occupied sites, for N up to 8. The numbers of attractors at fixed N and M agree with the expressions of the partition functions given in Table 1.

The exact rational values of the *a priori* densities $\rho_{N,*}$, defined in (72) in terms of the partition functions Z_N , and of the final densities $\rho_{N,\infty}$, defined in (89) in terms of the dynamical weights $W(\mathcal{C})$, are given in Table 3 and plotted against $1/N$ in Figure 7 for system sizes N up to 14, the largest system size for which the systematic enumeration approach has been carried out.

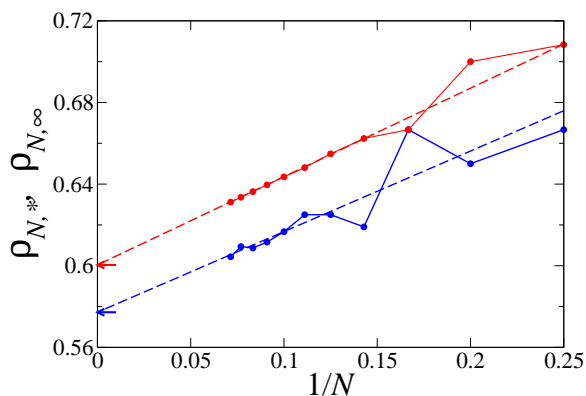


Fig. 7 Blue symbols: *a priori* densities $\rho_{N,*}$ defined in (72). Red symbols: final densities $\rho_{N,\infty}$ defined in (89). Data are taken from Table 3 and plotted against $1/N$, for sizes N ranging from 4 to 14. Arrows: respective limits ρ_* given in (78) and ρ_∞ given in Table 4. Dashed lines: guides to the eye demonstrating the asymptotic $1/N$ convergence of both datasets.

The complexity of the expressions of the final densities increases much faster than that of the *a priori* ones. This testifies the non-triviality of the dynamics of the Riviera model. Except for the system sizes $N = 1, 2, 3$ and 6, where all attractors have the same numbers of houses, respectively $M = 1, 2, 2$ and 4, the final density $\rho_{N,\infty}$ is larger than the *a priori* one by a few percent. This means that the dynamics of the Riviera model is able to

N	M	\mathcal{C}	$W(\mathcal{C})$
1	1	•	1
2	2	••	2
3	2	○••	2
		••○	2
		•○•	2
4	2	○••○	4
4	3	••••	10
		••○•	10
5	3	○••••	22
		••••○	22
		••○••	16
5	4	•••••	60
6	4	○•••••	142
		•••••○	142
		•○••••	106
		••○•••	106
		••••○•	144
		•••○••	80
7	4	○•••••○	280
		•••••○	280
		○••••••	318
		•••••○	318
		○•••••○	364
•••••○	272		
7	5	••••••	1158
		••••••	1158
		••••••	892
8	4	○•••••○	1120
8	5	○••••••	3114
		••••••	3114
		○••••••	3496
		••••••	3496
		•○••••	2386
		•••••○	2386
		••••••	2768
		••••••	2768
••••••	2464		
••••••	2464		
8	6	••••••	10744

Table 2 Dynamical weights $W(\mathcal{C})$ of all attractors of the Riviera model, ordered by increasing values of system size N and number M of occupied sites, for N up to 8.

reach on average slightly more compact configurations than a flat ensemble. We shall come back to this point in the Discussion.

For very large system sizes, the *a priori* densities $\rho_{N,\star}$ converge to the exactly known limit ρ_\star given in (78), whereas the final densities $\rho_{N,\infty}$ converge to the limit ρ_∞ , given in Table 4, which is only known through extensive numerical simulations. Figure 7 demonstrates that both datasets exhibit some irregular behavior for the smaller

N	$\rho_{N,\star}$	$\rho_{N,\infty}$
1	1	1
2	1	1
3	2/3	2/3
4	2/3	17/24
5	13/20	7/10
6	2/3	2/3
7	13/21	2921/4410
8	5/8	8801/13440
9	5/8	7559/11664
10	37/60	38921/60480
11	74/121	2340323/3659040
12	14/23	152397907/239500800
13	39/64	6410910971/10118908800
14	55/91	61139821/96864768

Table 3 Exact rational values of the *a priori* densities $\rho_{N,\star}$ defined in (72), and of the final densities $\rho_{N,\infty}$ defined in (89), for system sizes N up to 14.

sizes, and smoothly converge to their respective limits as $1/N$.

3.4 Numerical results in the thermodynamic limit

We end our investigation of the attractors of the Riviera model by describing the outcomes of extensive numerical simulations on systems of sizes $N = 100$ and 200 , comprising a total of 3.10^{12} sites. We have measured the final occupation correlation $C_{n,\infty}$ for distances n up to 13, beyond which the connected correlation is too small to be measured accurately.

Before we present numerical results, we wish to emphasize that the mean particle density and nearest-neighbor occupation correlation, i.e.,

$$C_{0,\infty} = \rho_\infty, \quad C_{1,\infty}, \quad (90)$$

can serve as a basis to express the main local observables characterizing the blocked configurations. First of all, the two local densities and the four nearest-neighbor correlations read

$$\begin{aligned}
\langle \bullet \rangle_\infty &= \rho_\infty, \\
\langle \circ \rangle_\infty &= 1 - \rho_\infty, \\
\langle \bullet \bullet \rangle_\infty &= C_{1,\infty}, \\
\langle \bullet \circ \rangle_\infty &= \langle \circ \bullet \rangle_\infty = \rho_\infty - C_{1,\infty}, \\
\langle \circ \circ \rangle_\infty &= C_{1,\infty} - 2\rho_\infty + 1.
\end{aligned} \quad (91)$$

Using the above expressions, we can prove that the identities (86) are constitutive to the model, by using only the local structure of the blocked configurations, as given by the patterns (55), as well as their translational invariance. We have indeed

$$\begin{aligned}
C_{2,\infty} &= \langle \bullet\bullet \rangle_\infty \\
&= \langle \bullet\circ \rangle_\infty - \langle \bullet\circ\circ \rangle_\infty \\
&= \langle \bullet\circ \rangle_\infty - \langle \circ\circ \rangle_\infty \\
&= 3\rho_\infty - 2C_{1,\infty} - 1, \\
C_{3,\infty} &= \langle \bullet\circ\circ \rangle_\infty + \langle \bullet\bullet\circ \rangle_\infty + \langle \bullet\circ\bullet \rangle_\infty \\
&= \langle \circ\circ \rangle_\infty + 2\langle \bullet\bullet\bullet \rangle_\infty \\
&= \langle \circ\circ \rangle_\infty + 2(\langle \bullet\circ\bullet \rangle_\infty - \langle \circ\bullet\circ \rangle_\infty) \\
&= 2\rho_\infty + C_{1,\infty} - 1. \tag{92}
\end{aligned}$$

The densities $\rho_\infty(\bullet)$ and $\rho_\infty(\bullet\bullet)$ of clusters of one and two consecutive occupied sites (houses) and the densities $\rho_\infty(\circ)$ and $\rho_\infty(\circ\circ)$ of clusters of one and two consecutive empty sites read

$$\begin{aligned}
\rho_\infty(\bullet) &= \rho_\infty - 2C_{1,\infty}, \\
\rho_\infty(\bullet\bullet) &= C_{1,\infty}, \\
\rho_\infty(\circ) &= 3\rho_\infty - 2C_{1,\infty} - 1, \\
\rho_\infty(\circ\circ) &= C_{1,\infty} - 2\rho_\infty + 1. \tag{93}
\end{aligned}$$

The total density of clusters of occupied (or empty) sites therefore reads

$$\begin{aligned}
\rho_\infty(\text{cl}) &= \rho_\infty(\bullet) + \rho_\infty(\bullet\bullet) \\
&= \rho_\infty(\circ) + \rho_\infty(\circ\circ) \\
&= \langle \bullet\circ \rangle_\infty = \langle \circ\bullet \rangle_\infty \\
&= \rho_\infty - C_{1,\infty}. \tag{94}
\end{aligned}$$

Table 4 gives the numerical values of the two basic observables introduced in (90), as well as those of the local observables given in (91), (93), (94). In these and subsequent numerical values, statistical errors are estimated to be of the order of 10^{-6} , i.e., one unit in the last significant digit.

Let us turn to the comparison of numerical data to the predictions of the *a priori* ensembles. The final density $\rho_\infty \approx 0.600385$ (see Table 4) is larger than the most probable density $\rho_\star \approx 0.577203$ in the full *a priori* ensemble (see (78))

ρ_∞	0.600385
$C_{1,\infty}$	0.237565
$\langle \bullet \rangle_\infty$	0.600385
$\langle \circ \rangle_\infty$	0.399615
$\langle \bullet\bullet \rangle_\infty$	0.237565
$\langle \bullet\circ \rangle_\infty$	0.362820
$\langle \circ\circ \rangle_\infty$	0.036795
$\rho_\infty(\bullet)$	0.125255
$\rho_\infty(\bullet\bullet)$	0.237565
$\rho_\infty(\circ)$	0.326025
$\rho_\infty(\circ\circ)$	0.036795
$\rho_\infty(\text{cl})$	0.362820

Table 4 Numerical values of the two basic observables introduced in (90) and of all local observables given in (91), (93), (94).

by a small but significant amount,

$$\rho_\infty - \rho_\star \approx 0.023182. \tag{95}$$

It is interesting to observe that ρ_\star is slightly below the middle of the range $[1/2, 2/3]$ of permitted densities, namely $\rho_{\text{mid}} = 7/12 \approx 0.583333$, whereas ρ_∞ is slightly larger than ρ_{mid} . These inequalities are rather general. We shall come back to this point in the Discussion (see (99) and Table 6).

The microcanonical *a priori* ensemble of blocked configurations whose mean density equals the final density ρ_∞ corresponds to the following values of the parameters u and x (see (61), (73), (76)):

$$u_\infty \approx 2.574600, \quad x_\infty \approx 4.602640. \tag{96}$$

The small density difference (95) translates into a sizeable difference between x_∞ and the value of x maximizing the configurational entropy, i.e., $x_\star = 1$ by construction. We nevertheless have $x_\infty < x_c$ (see (63)). The correlation $C_{n,\text{mic}}$ in the microcanonical ensemble at density ρ_∞ can be readily obtained for all distances n by inserting the value of u_∞ given in (96) into the initial values (85) and the recursion (84).

Table 5 presents a comparison between the numerical values of the final correlations $C_{n,\infty}$ and the exact microcanonical ones $C_{n,\text{mic}}$ for distances $n = 1, 2$ and 3, where correlations obey the identities (86). The differences $C_{n,\infty} - C_{n,\text{mic}}$, given in the last column, are very small. More importantly, they are found to be proportional to $+1, -2$ and

+1, in agreement with the identities (86). This parameter-free agreement to all significant digits provides a quantitative check of the accuracy of our numerical results.

n	$C_{n,\infty}$	$C_{n,\text{mic}}$	$C_{n,\infty} - C_{n,\text{mic}}$
1	0.237565	0.236440	+0.001125
2	0.326025	0.328275	-0.002250
3	0.438335	0.437210	+0.001125

Table 5 Numerical values of the final correlations $C_{n,\infty}$, exact microcanonical correlations $C_{n,\text{mic}}$, and differences $C_{n,\infty} - C_{n,\text{mic}}$, for distances $n = 1, 2$ and 3 , where correlations obey the identities (86).

Figure 8 shows a comparison between the final connected correlation $C_{n,\infty} - \rho_\infty^2$ (numerical values, red symbols) and its counterpart $C_{n,\text{mic}} - \rho_\infty^2$ in the microcanonical ensemble at fixed density ρ_∞ (exact values, blue symbols). Data are plotted on a logarithmic scale against distance n . Full (resp. empty) symbols denote positive (resp. negative) connected correlations. The microcanonical connected correlations exhibit everlasting irregular oscillations on this logarithmic scale, whose hull falls off exponentially with decay rate (inverse correlation length)

$$\mu_{\text{mic}} = \frac{1}{2} \ln u_\infty \approx 0.472847 \quad (97)$$

(blue dashed line), as predicted in (88). The final connected correlations exhibit smaller oscillations, except for an outlier at distance 5. These oscillations seem to be damped on this logarithmic scale, in the sense that their amplitude exhibits a slow decay, at variance with the microcanonical ones. Their hull is observed to fall off roughly twice faster, with an apparent decay rate

$$\mu_\infty \approx 0.81 \quad (98)$$

(red dashed line). The observed period three in the signs of final connected correlations is probably a transient phenomenon with no intrinsic meaning.

4 Discussion

The goal of the present paper was twofold. We have given a concise review of the theory of one-dimensional spin models with kinetic constraints,

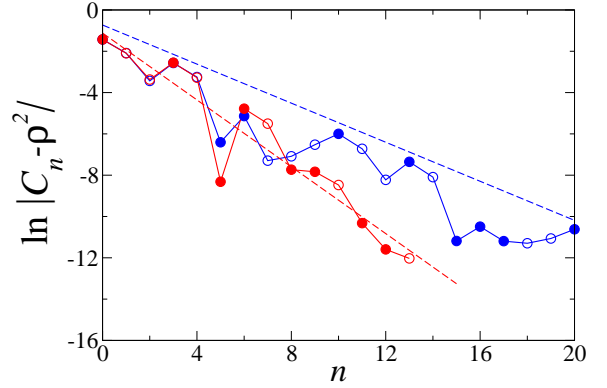


Fig. 8 Comparison between the final connected correlation $C_{n,\infty} - \rho_\infty^2$ (numerical values, red symbols) and its counterpart $C_{n,\text{mic}} - \rho_\infty^2$ in the microcanonical *a priori* ensemble at fixed density ρ_∞ (exact values, blue symbols). Data are plotted on a logarithmic scale against distance n . Full (resp. empty) symbols denote positive (resp. negative) connected correlations. The blue dashed line has the exact slope (97). The red dashed with slope 0.81 is the outcome of a least-square fit.

exemplified by the case of the constrained Ising chain, and put this body of knowledge in perspective with a range of novel results on the Riviera model introduced recently by Puljiz et al. [50].

This work has evidenced that there are both significant analogies and differences between the one-dimensional kinetically constrained models whose fully irreversible zero-temperature dynamics can be mapped onto an RSA model, and the Riviera model, whose fully irreversible dynamics does not enjoy the characteristic shielding property of those RSA models. It is worth noticing that the bilateral avatar of the Riviera model, defined by the requirement that *both* neighboring plots of each house should remain forever unbuilt, amounts to a deposition model with excluded volume described in [45]. The latter model is equivalent to the dimer deposition model on the dual lattice. It therefore belongs to the above class of kinetically constrained models.

Among the common features shared by the Riviera model and the class of RSA models, we wish to underline that the final particle density ρ_∞ , i.e., the particle density of the attractors reached by the dynamics, is slightly different from the most probable density ρ_* in the full *a priori* ensemble of blocked configurations. One can therefore speak of a universally weak violation of the Edwards flatness hypothesis. In most cases we

Number	Model	ρ_{\min}	ρ_{\max}	ρ_{mid}	ρ_{\star}	ρ_{∞}
1	Riviera	0.5	0.666666	0.583333	0.577203	0.600385
2	Dimers	0.666666	1	0.833333	0.822991	0.864664
3	Ising-Glauber	0.5	1	0.75	0.723607	0.816060
4	Ising-Kawasaki	0.333333	1	0.666666	0.618420	<i>0.637043</i>
5	Paramagnetic Ising	0.5	1	0.75	0.723607	<i>0.696734</i>

Table 6 Various characteristic densities for the Riviera model and four kinetically constrained Ising chains whose dynamics can be mapped onto an RSA model: ρ_{\min} and ρ_{\max} are the endpoints of the range of permitted densities, ρ_{mid} is the midpoint of the latter range, ρ_{\star} is the most probable density in the full *a priori* statistical ensemble, ρ_{∞} is the final density of the attractors of the irreversible dynamics launched from a prescribed initial state, be it either empty or corresponding to infinite temperature (see text for details). All data obey the inequalities (99), except the last two entries of the rightmost column (slanted numbers).

have

$$\rho_{\star} < \rho_{\text{mid}} < \rho_{\infty}, \quad (99)$$

where $\rho_{\text{mid}} = (\rho_{\min} + \rho_{\max})/2$ is the midpoint of the range of permitted densities. The above rule of thumb expresses that the statistical ensemble tends to favor lower-density blocked configurations, whereas the dynamics tends to favor higher-density blocked configurations. This is illustrated by Table 6, giving the values of ρ_{\min} , ρ_{\max} , ρ_{mid} , ρ_{\star} and ρ_{∞} for the Riviera model and four characteristic one-dimensional kinetic spin models whose zero-temperature dynamics can be mapped onto an RSA model. The detailed contents of Table 6 are as follows. Model 1 is the Riviera model, investigated extensively in Section 3. The exact value of ρ_{\star} and the numerical value of ρ_{∞} are respectively given in (78) and in Table 4. For the four subsequent models, both ρ_{\star} and ρ_{∞} are known exactly. Model 2 is the problem of dimer deposition. The value of ρ_{\star} is not related to (23), because here the system is assumed to be initially empty [56]. The value of ρ_{∞} is the celebrated result of Flory (see (41)). The last three models concern the Ising chain with an infinite-temperature initial state. Model 3 is the ferromagnetic Ising chain with kinetically constrained zero-temperature Glauber dynamics, investigated extensively in Section 2 (see (23) and (43), with $E = 1 - 2\rho$). Model 4 is the ferromagnetic Ising chain with kinetically constrained zero-temperature Kawasaki dynamics [26–30], whereas model 5 is the paramagnetic Ising chain in a uniform magnetic field subjected to zero-temperature either symmetrically or asymmetrically constrained dynamics [23–25]. In the

last two cases, the final density ρ_{∞} (slanted numbers) is smaller than ρ_{mid} and therefore does not obey the inequality (99).

The most salient qualitative difference between the Riviera model and the kinetically constrained models in the RSA class concerns their final correlation functions. This unlikeness was somewhat to be expected, since the Riviera model does not enjoy the shielding property. The numerical data shown in Figure 8 strongly suggest that the connected correlation function $C_{n,\infty} - \rho_{\infty}^2$ falls off exponentially, with a decay rate $\mu \approx 0.81$ (see (98)). This observed exponential decay is in stark contrast with the superexponential, inverse-factorial decay of connected correlations that is universally met in one-dimensional RSA models. Exponentially decaying correlations are rather viewed as a characteristic of either thermal or otherwise equilibrated systems. From this viewpoint the Riviera model thus appears as a chimera with, on the one hand, a fully irreversible dynamics leading to metastability with an exponentially large number of attractors and, on the other hand, exponentially decaying correlations germane to those observed at thermal equilibrium.

Acknowledgments

It is a pleasure to dedicate this paper to our colleague and friend Malte Henkel on the occasion of his 60th birthday. We acknowledge with thanks useful exchanges with Mate Puljiz, Stjepan Šebek and Josip Žubričić.

Author contribution statement

Both authors contributed equally to the present work, were equally involved in the preparation of the manuscript, and have read and approved the final manuscript.

Data availability statement

Data sharing not applicable to this article as no datasets were generated or analysed during the current study.

References

- [1] Goldstein, M.: Viscous liquids and the glass transition: a potential energy barrier picture. *J. Chem. Phys.* **51**, 3728–3739 (1969)
- [2] Thouless, D.J., Anderson, P.W., Palmer, R.G.: Solution of ‘solvable model of a spin glass’. *Phil. Mag.* **35**, 593–601 (1977)
- [3] Kirkpatrick, S., Sherrington, D.: Infinite-ranged models of spin-glasses. *Phys. Rev. B* **17**, 4384–4403 (1977)
- [4] Mézard, M., Parisi, G., Virasoro, M.A.: *Spin Glass Theory and Beyond*. World Scientific, Singapore (1986)
- [5] Götze, W., Sjögren, L.: Relaxation processes in supercooled liquids. *Rep. Prog. Phys.* **55**, 241–376 (1992)
- [6] Gaveau, B., Schulman, L.S.: Theory of nonequilibrium first-order phase transitions for stochastic dynamics. *J. Math. Phys.* **39**, 1517–1533 (1998)
- [7] Biroli, G., Monasson, R.: From inherent structures to pure states: some simple remarks and examples. *Europhys. Lett.* **50**, 155–161 (2000)
- [8] Debenedetti, P.G., Stillinger, F.H.: Supercooled liquids and the glass transition. *Nature* **410**, 259–267 (2001)
- [9] Berthier, L., Biroli, G.: Theoretical perspective on the glass transition and amorphous materials. *Rev. Mod. Phys.* **83**, 587–645 (2011)
- [10] Biroli, G., Garrahan, J.P.: Perspective: the glass transition. *J. Chem. Phys.* **138**, 12–301 (2013)
- [11] Spirin, V., Krapivsky, P.L., Redner, S.: Fate of zero-temperature Ising ferromagnets. *Phys. Rev. E* **63**, 036118 (2001)
- [12] Spirin, V., Krapivsky, P.L., Redner, S.: Freezing in Ising ferromagnets. *Phys. Rev. E* **65**, 016119 (2001)
- [13] Barros, K., Krapivsky, P.L., Redner, S.: Freezing into stripe states in two-dimensional ferromagnets and crossing probabilities in critical percolation. *Phys. Rev. E* **80**, 040101 (2009)
- [14] Olejarz, J., Krapivsky, P.L., Redner, S.: Fate of 2d kinetic ferromagnets and critical percolation crossing probabilities. *Phys. Rev. Lett.* **109**, 195702 (2012)
- [15] Olejarz, J., Krapivsky, P.L., Redner, S.: Zero-temperature relaxation of three-dimensional Ising ferromagnets. *Phys. Rev. E* **83**, 051104 (2011)
- [16] Glauber, R.J.: Time-dependent statistics of the Ising model. *J. Math. Phys.* **4**, 294–307 (1963)
- [17] Bray, A.J.: Theory of phase-ordering kinetics. *Adv. Phys.* **43**, 357–459 (1994)
- [18] Cornell, S.J., Kaski, K., Stinchcombe, R.B.: Domain scaling and glassy dynamics in a one-dimensional Kawasaki Ising model. *Phys. Rev. B* **44**, 12263–12274 (1991)
- [19] De Smedt, G., Godrèche, C., Luck, J.M.: Metastable states of the Ising chain with Kawasaki dynamics. *Eur. Phys. J. B* **32**, 215–225 (2003)
- [20] Derrida, B., Gardner, E.: Metastable states of a spin glass chain at 0 temperature. *J. Phys. (France)* **47**, 959–965 (1986)
- [21] Masui, S., Southern, B.W., Jacobs, A.E.: Metastable states of Ising spin glasses and random ferromagnets. *Phys. Rev. B* **39**, 124401 (1989)

- 6925–6933 (1989)
- [22] Ritort, F., Sollich, P.: Glassy dynamics of kinetically constrained models. *Adv. Phys.* **52**, 219–342 (2003)
- [23] Fredrickson, G.H., Andersen, H.C.: Kinetic Ising model of the glass transition. *Phys. Rev. Lett.* **53**, 1244–1247 (1984)
- [24] Jäckle, J., Eisinger, S.: A hierarchically constrained kinetic Ising model. *Z. Phys. B* **84**, 115–124 (1991)
- [25] Sollich, P., Evans, M.R.: Glassy time-scale divergence and anomalous coarsening in a kinetically constrained spin chain. *Phys. Rev. Lett.* **83**, 3238–3241 (1999)
- [26] Palmer, R.G., Frisch, H.L.: Low-and high-dimension limits of a phase separation model. *J. Stat. Phys.* **38**, 867–872 (1985)
- [27] Elskens, Y., Frisch, H.L.: Aggregation kinetics for a one-dimensional zero-degree Kelvin model of spinodal decomposition. *J. Stat. Phys.* **48**, 1243–1248 (1987)
- [28] Privman, V.: Exact solution of a phase separation model with conserved order parameter dynamics. *Phys. Rev. Lett.* **69**, 3686–3688 (1992)
- [29] Lin, J.C., Taylor, P.L.: Exact solution of a phase-separation model with conserved-order-parameter dynamics and arbitrary initial concentration. *Phys. Rev. E* **48**, 4305–4308 (1993)
- [30] Krapivsky, P.L.: Kinetic models of a binary alloy at zero temperature. *J. Stat. Phys.* **74**, 1211–1225 (1994)
- [31] Dean, D.S., Lefèvre, A.: Tapping spin glasses and ferromagnets on random graphs. *Phys. Rev. Lett.* **86**, 5639–5642 (2001)
- [32] Dean, D.S., Lefèvre, A.: Steady state behavior of mechanically perturbed spin glasses and ferromagnets. *Phys. Rev. E* **64**, 046110 (2001)
- [33] Lefèvre, A., Dean, D.S.: Tapping thermodynamics of the one-dimensional Ising model. *J. Phys. A: Math. Gen.* **34**, L213–L220 (2001)
- [34] Prados, A., Brey, J.J.: Analytical solution of a one-dimensional Ising model with zero-temperature dynamics. *J. Phys. A: Math. Gen.* **34**, L453–L459 (2001)
- [35] De Smedt, G., Godrèche, C., Luck, J.M.: Jamming, freezing and metastability in one-dimensional spin systems. *Eur. Phys. J. B* **27**, 363–380 (2002)
- [36] Godrèche, C., Luck, J.M.: Metastability in zero-temperature dynamics: statistics of attractors. *J. Phys.: Condens. Matter* **17**, 2573–2590 (2005)
- [37] Jäckle, J.: On the glass transition and the residual entropy of glasses. *Phil. Mag.* **44**, 533–545 (1981)
- [38] Palmer, R.G.: Broken ergodicity. *Adv. Phys.* **31**, 669–735 (1982)
- [39] Krapivsky, P.L., Luck, J.M. in preparation.
- [40] Edwards, S.F.: The role of entropy in the specification of a powder. In: Mehta, A. (ed.) *Granular Matter: an Interdisciplinary Approach*. Springer, New York (1994)
- [41] Edwards, S.F., Mehta, A.: Dislocations in amorphous materials. *J. Phys. (France)* **50**, 2489–2503 (1989)
- [42] Mehta, A., Edwards, S.F.: Statistical mechanics of powder mixtures. *Physica A* **157**, 1091–1100 (1989)
- [43] Edwards, S.F., Oakeshott, R.B.S.: Theory of powders. *Physica A* **157**, 1080–1090 (1989)
- [44] Baule, A., Morone, F., Herrmann, H.J., Makse, H.A.: Edwards statistical mechanics for jammed granular matter. *Rev. Mod. Phys.* **90**, 015006 (2018)
- [45] Evans, J.W.: Random and cooperative sequential adsorption. *Rev. Mod. Phys.* **65**, 1281–1329 (1989)

- [46] Talbot, J., Tarjus, G., Van Tassel, P.R., Viot, P.: From car parking to protein adsorption: an overview of sequential adsorption processes. *Colloids Surfaces A* **165**, 287–324 (2000)
- [47] Krapivsky, P.L., Redner, S., Ben-Naim, E.: *A Kinetic View of Statistical Physics*. Cambridge University Press, Cambridge (2010)
- [48] Flory, P.J.: Intramolecular reaction between neighboring substituents of vinyl polymers. *J. Am. Chem. Soc.* **61**, 1518–1521 (1939)
- [49] Rényi, A.: On a one-dimensional problem concerning random space-filling. *Publ. Math. Inst. Hung. Acad. Sci.* **3**, 109–127 (1958)
- [50] Došlić, T., Puljiz, M., Šebek, S., Žubrinić, J.: On a variant of the Flory model. arXiv:2210.12411 (2022)
- [51] Puljiz, M., Šebek, S., Žubrinić, J.: Combinatorial settlement planning. *Contrib. Discrete Math.* (to appear). arXiv:2107.07555
- [52] Puljiz, M., Šebek, S., Žubrinić, J.: Packing density of combinatorial settlement planning models. arXiv:2107.09417 (2021)
- [53] Evans, J.W., Burgess, D.R., Hoffman, D.K.: Irreversible random and cooperative processes on lattices: Spatial correlations. *J. Math. Phys.* **25**, 3051–3063 (1984)
- [54] Monthus, C., Hilhorst, H.J.: The pair correlation function in a randomly sequentially filled one-dimensional lattice. *Physica A* **175**, 263–274 (1991)
- [55] Pedersen, F.B., Hemmer, P.C.: Time evolution of correlations in a random sequential adsorption process. *J. Chem. Phys.* **98**, 2279–2282 (1993)
- [56] Krapivsky, P.L.: Large deviations in one-dimensional random sequential adsorption. *Phys. Rev. E* **102**, 062108 (2020)
- [57] OEIS: The On-Line Encyclopedia of Integer Sequences. <https://oeis.org>
- [58] Allen, M.A., Edwards, K.: Connections between two classes of generalized Fibonacci numbers squared and permanents of $(0,1)$ Toeplitz matrices. *Linear and Multilinear Algebra*, 1–13 (2022)
- [59] Krapivsky, P.L., Luck, J.M.: Coverage fluctuations in theater models. *J. Stat. Mech.* 063209 (2019)